other interpenetrating structures, interweaving in MOFs with a framework conforming closely to a periodic minimal surface can produce materials with large cavities, exceptionally high pore volume, and permanent porosity, as exemplified by MOF-14.

References and Notes

1. J. P. Sauvage, C. Dietrich-Buchecker, Eds., *Molecular Catenanes, Rotaxanes and Knots* (Wiley-VCH, New York, 1999).
2. F. M. Raymo, J. F. Stoddart, *Chem. Rev.* **99**, 1643 (1999).
3. N. C. Seeman, *Annu. Rev. Biophys. Biomol. Struct.* **27**, 225 (1998).
4. J. J. Storhoff, C. A. Mirkin, *Chem. Rev.* **99**, 1849 (1999).
5. W. R. Wikoff *et al.*, *Science* **289**, 2129 (2000).
6. S. R. Batten, R. Robson, *Angew. Chem. Int. Ed.* **37**, 1460 (1998).
7. For the design of intergrown nets with optimal porosity, see T. M. Reineke, M. Eddaoudi, D. Moler, M. O'Keeffe, O. M. Yaghi, *J. Am. Chem. Soc.* **122**, 4843 (2000).
8. M. O'Keeffe, M. Eddaoudi, H. Li, T. Reineke, O. M. Yaghi, *J. Solid State Chem.* **152**, 3 (2000).
9. M. O'Keeffe, B. G. Hyde, *Crystal Structures I: Patterns and Symmetry* (Mineralogical Society of America, Washington, DC, 1996).
10. S. T. Hyde *et al.*, *The Language of Shape* (Elsevier, Amsterdam, 1997).
11. The vertices of two interpenetrating diamond nets form the dense body-centered cubic array as in the structures of NaTl compounds [see, e.g., (*8*)].
12. For a recent example and references, see B. Chen *et al.*, *J. Am. Chem. Soc.* **122**, 11559 (2000).
13. Details of the elemental analysis and crystal structures for as-synthesized and evacuated MOF-14 [$Im\bar{3}$, a = 26.946(2) and 26.919(1) Å, respectively] and the elemental analysis of solvent-exchanged MOF-14 are available at *Science* Online (www.sciencemag.org/cgi/content/full/291/5506/1021/DC1). X-ray coordinates have been deposited with the Cambridge Data Bank.
14. E. Weber *et al.*, *J. Chem. Soc. Perkin Trans. II* **1988**, 1251 (1988).
15. H. Li, M. Eddaoudi, M. O'Keeffe, O. M. Yaghi, *Nature* **402**, 276 (1999).
16. M. Eddaoudi, H. Li, O. M. Yaghi, *J. Am. Chem. Soc.* **122**, 1391 (2000).
17. D. W. Breck, *Zeolite Molecular Sieves* (Wiley, New York, 1974).

18. Supported by NSF grants DMR-9804817 (M.O'K.) and CHE-9980469 (O.M.Y.) and by the U.S. Department of Energy (O.M.Y.). We thank S. Ramsden for production of Fig. 2.

16 October 2000; accepted 21 December 2000

Surface-Directed Liquid Flow Inside Microchannels

Bin Zhao,[1] Jeffrey S. Moore,[1]* David J. Beebe[2]

Self-assembled monolayer chemistry was used in combination with either multistream laminar flow or photolithography to pattern surface free energies inside microchannel networks. Aqueous liquids introduced into these patterned channels are confined to the hydrophilic pathways, provided the pressure is maintained below a critical value. The maximum pressure is determined by the surface free energy of the liquid, the advancing contact angle of the liquid on the hydrophobic regions, and the channel depth. Surface-directed liquid flow was used to create pressure-sensitive switches inside channel networks. The ability to confine liquid flow inside microchannels with only two physical walls is expected to be useful in applications where a large gas-liquid interface is critical, as demonstrated here by a gas-liquid reaction.

Manipulating gas and liquid fluids within networks of microchannels is crucial in the design and fabrication of microfluidic devices for applications in bioassays, microreactors, and chemical and biological sensing (*1*). Many techniques including mechanical pumping (*2*), electro-osmotic flow (*3, 4*), electrowetting (*5*), electrochemistry (*6*), and thermocapillary pumping (*7, 8*) have been used to pump, transport, position, and mix liquid samples. Surface properties, especially wetting, have significant effects on liquid behavior (*9–11*) when the system is reduced to a submillimeter scale. For example, surface effects are the basis of capillary pumping (*12*) and light-driven motion of liquids on a photoresponsive surface (*13*). Recent studies on patterned surfaces (*14–16*) revealed interesting phenomena that can be exploited to control liquid motions in microfluidic devices. Here, we report a simple method, based on patterning surface free energies, to manipulate liquid flow within channel networks. Aqueous solutions are confined to hydrophilic pathways, creating a large gas-liquid interface that makes gas-liquid reactions practical in microfluidic systems.

Patterning hydrophobic and hydrophilic regions inside microchannels typically requires modifying the surface in selected areas first, and then aligning and bonding substrates to form microchannel networks (*11*). This process consists of a series of complicated and time-consuming steps. We have patterned surface free energies inside channel networks by combining multistream liquid laminar flow and self-assembled monolayer (SAM) chemistry. The entire process is completed quickly (within several minutes) and in situ. Liquid flow inside microchannels is laminar, meaning that multiple liquid streams can flow side-by-side without turbulent mixing, allowing good spatial control (*17*). Multistream liquid laminar flow has been used to fabricate diffusion-based extractors, various microstructures, and cell patterns inside preformed capillaries (*17–20*). Deposition of SAMs is a simple method to modify surface wetting properties of a variety of materials (*21–23*). By controlling the water content in the solvent, SAMs of trichlorosilanes can be formed on silica substrates in a short period of time (i.e., several minutes or even less) (*22, 24*).

The channels used here were made from glass substrates and glass cover slips (*25*). A stream of pure hexadecane and a stream of octadecyltrichlorosilane (OTS) solution in hexadecane were brought together in channels by syringe pumps, and the laminar flow was maintained for 2 to 3 min (*26*). SAMs formed on both the top and bottom of the channels in the area containing the trichlorosilane solution. The other surfaces remained hydrophilic ($\theta_p \sim 0°$; θ_p is the water advancing contact angle on a polar surface). A series of patterned surfaces were fabricated as shown in Fig. 1, A to D. Once patterned, aqueous solutions flowed only on hydrophilic pathways (Fig. 1, E to H, corresponding to Fig. 1, A to D, respectively) when the pressure was maintained below a critical value. If minor disturbances caused the liquid to flow into the hydrophobic region, the liquid gradually retreated to the hydrophilic pathway. When the pressure exceeded a critical value, the solution crossed the boundary between hydrophilic and hydrophobic regions. Using these patterned surfaces, we could transport liquids from one reservoir to another along the specified pathway (Fig. 1F), and could flow two streams side-by-side separated by a gas membrane, allowing volatile compounds to be transported from one stream to the other (Fig. 1, E, G, and H). Because there are no physical walls on the sides of the liquid stream, we refer to the stream as being confined by "virtual" walls.

A liquid stream will rupture the virtual wall when the angle of curvature of the liquid at the hydrophilic-hydrophobic boundary (θ_b) equals the advancing contact angle of the liquid on the nonpolar surface (θ_n) (Fig. 2A). When the water surface is curved, there is a pressure drop across the liquid-gas interface due to surface free energy. The pressure on the concave side is always greater than the pressure on the convex side, as described by the Young-Laplace equation $\Delta P = \gamma(1/R_1 +$

[1]The Beckman Institute for Advanced Science and Technology, University of Illinois at Urbana-Champaign, Urbana, IL 61801, USA. [2]Department of Biomedical Engineering, University of Wisconsin–Madison, Madison, WI 53706, USA.

*To whom correspondence should be addressed. E-mail: moore@scs.uiuc.edu

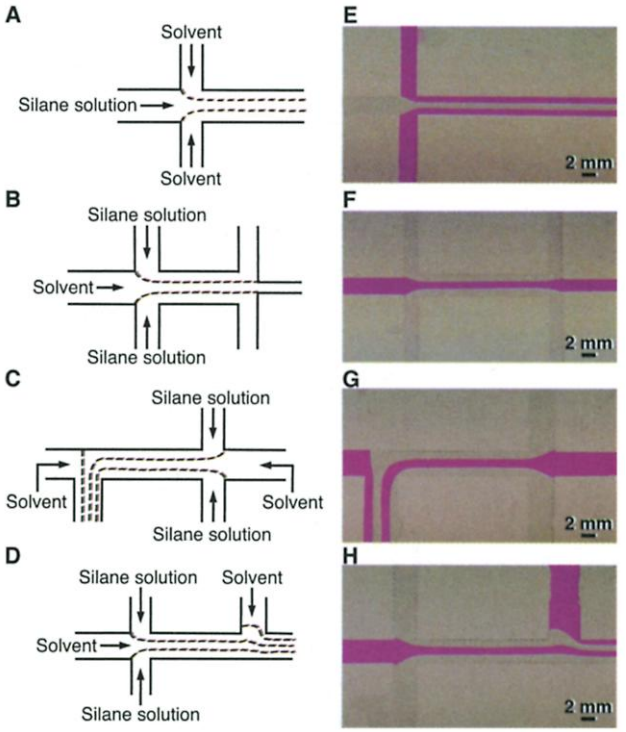

Fig. 1. Schematic illustrations of multistream laminar flows (**A** to **D**) and the corresponding images of aqueous flow inside channels after surface patterning (**E** to **H**). The liquid is a dilute solution of Rhodamine B dye (0.057 w/w %) in deionized water.

$1/R_2$) (*9*), where ΔP is the pressure difference, γ is the liquid surface free energy, and R_1 and R_2 are the radii of curvature in directions vertical and parallel, respectively, to the liquid stream. For a straight stream (Fig. 1F), R_2 is infinite and the equation is simplified to $\Delta P = \gamma/R_1$. The value R_1 can be expressed by the equation $R_1 = h/[2\sin(\theta_b - 90°)]$, where h is the channel depth. Based on the essential condition for virtual wall rupture ($\theta_b = \theta_n$), the maximum pressure that virtual walls in a straight stream can sustain is $P_{max} = \Delta P = (2\gamma/h)\sin(\theta_n - 90°)$. Thus, the virtual walls cannot withstand any pressure if $\theta_n < 90°$. Experimentally, we have confirmed this prediction by using bromoundecyltrichlorosilane instead of OTS to modify surface wetting property ($\theta_n = 83°$). Carefully adding deionized water into the channel initially resulted in water being confined to the hydrophilic regions, but a slight pressure increase caused water to cross the boundary and rupture the virtual walls.

The channel depth used here is ~180 μm and the θ_n of water on a SAM of OTS is 112°. Calculations show that P_{max} is 300 N/m^2, corresponding to a pressure of 30.6 mm of water (mmH_2O). For a SAM of heptadecafluoro-1,1,2,2-tetrahydrodecyltrichlorosilane (HFTS), the θ_n of deionized water is 118°, corresponding to a critical pressure of 376 N/m^2 (38.4 mmH_2O). We used the design in Fig. 1F to measure P_{max} for surfaces patterned with these two trichlorosilanes. Although the measurement was complicated by kinetic issues and high humidity inside the channels, we observed that bulges developed at a pressure of 31 mmH_2O for OTS-patterned channels and 37 mmH_2O for HFTS-patterned channels (*27*), in good agreement with our analytical predictions.

On the basis of the maximum pressure differences for the OTS and HFTS monolayers, we designed and fabricated simple pressure-sensitive switches to direct the flow of liquids inside channel networks (Fig. 3). The central region was hydrophilic, whereas the other two parts were modified with SAMs of OTS and HFTS, respectively. Therefore, the maximum pressures that the two virtual walls of the liquid stream can sustain are different. At a low pressure [for example, 10 mmH_2O (Fig. 3B)], the aqueous Rodamine B solution flowed only along the central hydrophilic pathway from (a) to (b). At a medium pressure $P_{OTS} < P < P_{HFTS}$ [Fig. 3C, 26 mmH_2O (*28*)] the virtual wall between the hydrophilic and OTS regions ruptured and water flowed from (a) to (b), (c), and (d). At a higher pressure $P > P_{HFTS}$ (Fig. 3D), aqueous solution flowed through all channels from (a) to (b), (c), (d), (e), and (f). Because the contact angle can be systematically adjusted by using mixed SAMs of two different trichlorosilanes, the liquid flow direction can be switched at any desired pressure.

The previous discussion is for a straight stream. If there is a turn in the hydrophilic pathway (Fig. 1G), R_2 is finite. For the outer virtual wall of the turn, R_2 is positive and P_{max} increases. For the inner virtual wall, R_2 is negative, lowering P_{max}. Thus, there is a limit on the sharpness of turns that can be

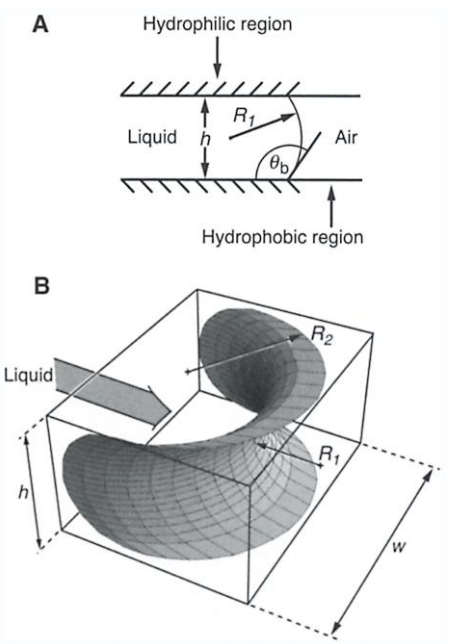

Fig. 2. (**A**) Angle of curvature θ_b of a liquid confined by a virtual wall inside a microchannel. (**B**) Schematic illustration of the tip of a liquid advancing through a surface-defined pathway. The top and bottom are hydrophilic glass substrates; the hydrophobic virtual walls are on the sides.

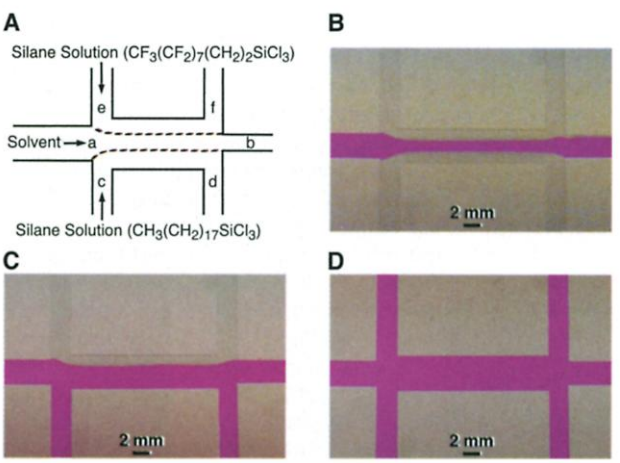

Fig. 3. Pressure-sensitive valves. (**A**) The laminar flow scheme for patterning surface free energies inside channels with two different trichlorosilanes, OTS and HFTS. (**B** through **D**) Images of flow patterns of a Rhodamine B dilute solution are shown at various pressures (expressed as water column height, or mmH_2O): (B) 10 mm, (C) 26 mm, and (D) 39 mm. The concentration of dye in deionized water is 0.057 w/w %.

introduced without the liquid crossing the boundary. When R_1 is equal to R_2 but opposite in sign, $\Delta P = 0$. Therefore the critical value of R_2 is $h/[2\sin(\theta_n - 90°)]$. Similar considerations allow us to predict the critical geometry of pathways that will support spontaneous liquid flow. Figure 2B illustrates the tip of an advancing aqueous stream confined by two hydrophilic physical walls separated by distance h and two hydrophobic virtual walls spaced by width w. The capillary force generated by the hydrophilic surfaces produces a side-view profile with a negative R_1, whereas the retraction force from the hydrophobic virtual walls causes a top-view profile with a positive R_2. If $|R_2| > |R_1|$, $\Delta P < 0$ and water spontaneously wets the hydrophilic pathway. If $|R_2| < |R_1|$, $\Delta P > 0$ and water does not spontaneously flow through the hydrophilic region. The critical condition for spontaneous flow occurs when R_2 is equal to R_1, that is, when $w \geq h/(\cos\theta_p)$. For $\theta_p = 0°$, the critical width of the stream is equal to the channel depth. A higher contact angle (but with $\theta_p < 90°$) in the hydrophilic pathway requires a larger width for flow to take place spontaneously.

Pattern formation achieved by multistream liquid laminar flow requires preformed channel networks, limiting the use of surface-directed liquid flow in device applications. To overcome these limitations, we developed a photolithographic method to pattern surface free energies inside microchannels. Using the photochemistry of the 2-nitrobenzyl group (*29*), we designed and synthesized the photocleavable SAMs shown in Fig. 4A. Ultraviolet (UV) irradiation through masks placed on top of SAM-modified channels led to the production of hydrophilic carboxylate groups in the irradiated regions (Fig. 4B). Once photopatterned, aqueous solutions were confined to the irradiated regions. It is evident that there is good fidelity in the transfer of the pattern from the mask to the liquid pathway (Fig. 4, C and D). This photopatterning method provides greater flexibility in the design and generation of complex flow patterns and facilitates mass manufacturing of surface-directed flow devices.

Virtual walls provide a large gas-liquid interface that allows a practical means to perform gas-liquid reactions in microchips. Figure 5 demonstrates a gas-liquid reaction. The aqueous solution confined in the hydrophilic pathway consists of a pH = 6.44 phosphate buffer solution containing the acid-base indicator methyl red. When acetic acid vapor was carried into the channels by a nitrogen stream, a reaction occurred with the buffer causing the solution's color to change from light yellow to pink. Under our experimental conditions, the diffusion was rapid, as revealed by the velocity of the pink frontline. Gas-liquid and gas-solid interactions are critical in the detection of biological and chemical agents. Virtual walls offer a new approach for these types of analyses, and with appropriate design, may enable high sensitivity to be achieved in a portable monitor.

By taking advantage of the large interface

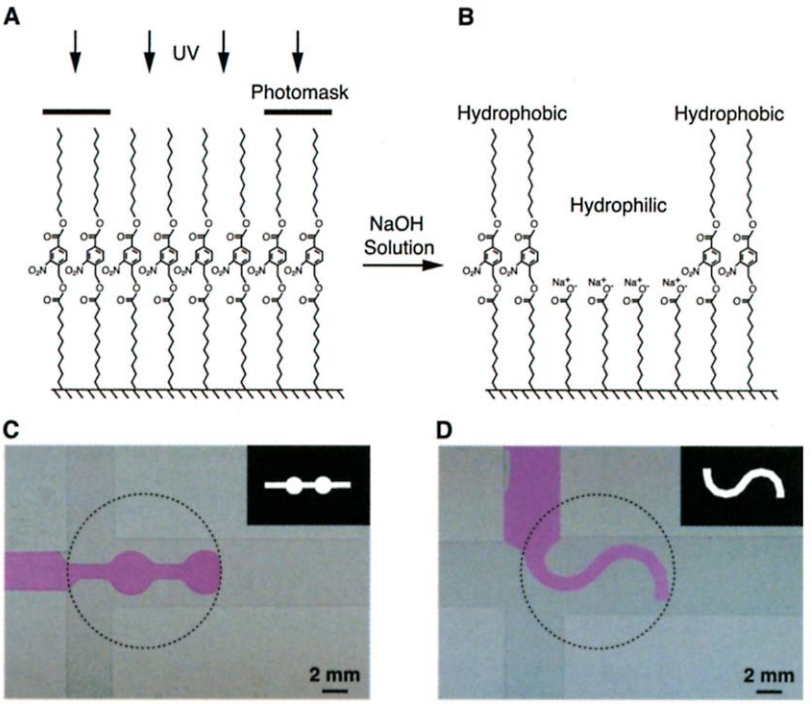

Fig. 4. Ultraviolet photopatterning to fabricate hydrophilic and hydrophobic surface patterns inside microchannels. (**A**) The molecular structure of a photocleavable SAM formed on glass surfaces. The microchannels were cleaned by sequentially flushing with 10 ml of hexane and 10 ml of methanol after monolayer deposition from a 0.5 w/w % solution of the corresponding trichlorosilane in hexadecane, and then dried with a stream of nitrogen. A photomask was placed on top of the SAM-coated channel filled with pH = 11.77 NaOH solution. The UV light source was an Olympus Epi-Fluorescent Microscope (BX-60) passed through a near-UV filter cube (U-MNUA, type BP 360-370 nm) with a band pass of 360- to 370-nm wavelength. A 2× magnification lens was used, and the irradiation time was 90 min. After irradiation, the channel was rinsed with 10 ml of methanol and then dried with a stream of clean air. (**B**) Schematic illustration of the molecular structures in irradiated and unirradiated regions. (**C** and **D**) A dilute Rhodamine B aqueous solution was added into the channels by a syringe, and a pressure was applied to push the solution slowly through the hydrophobic region. When the aqueous solution reached the edge of the irradiated area, it wetted the hydrophilic region spontaneously and formed patterns identical to the photomasks, shown at a reduced size in the upper right corner. The circle represents the size of the UV-exposed region.

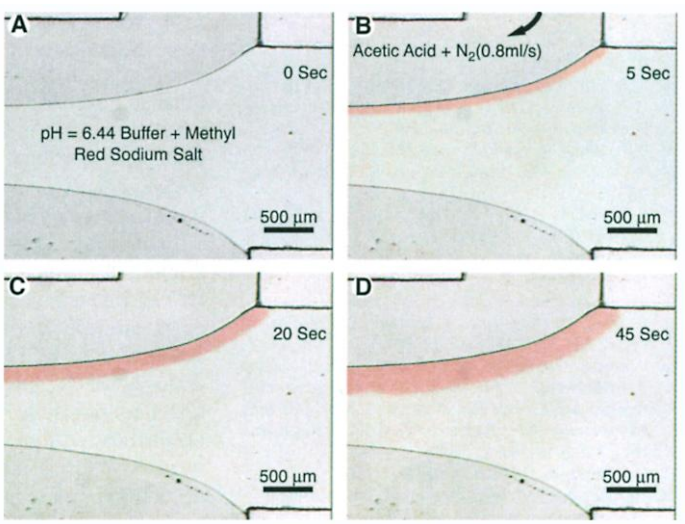

Fig. 5. Optical micrographs of a gas-liquid reaction. The liquid was a pH = 6.44 phosphate buffer solution containing the acid-base indicator methyl red (the concentration of methyl red sodium salt in buffer solution is 0.007 w/w %). Acetic acid vapor was carried into the channel by bubbling N_2 through glacial acetic acid. The flow rate of nitrogen was 0.8 ml/s as measured by a Hewlett-Packard soap film flowmeter. Shown are micrographs of the channel (**A**) before acetic acid vapor was introduced into the channel (0 s), and at (**B**) 5 s, (**C**) 20 s, and (**D**) 45 s after initiating flow of acetic acid vapor.

of virtual walls, we can produce functionality on microchips that is difficult to realize by other methods. For example, concentrating samples in microfluidic systems is nontrivial. Methods reported include sample stacking using "isoelectric focusing" (*30*) and on-chip solid phase extraction (*31*). The virtual walls provide an intuitive method to concentrate liquids on microchips. Virtual walls can also mimic the function of lungs by exchanging components between liquid and gas phases. In combination with in situ–constructed stimuli-responsive hydrogel components (*25, 32*), more complex functions could be added to realize even greater control in microfluidic systems. We believe that the approaches we describe provide enhanced functionality and design flexibility that expand the toolbox for the design and fabrication of microfluidic systems.

References and Notes

1. M. Freemantle, *Chem. Eng. News* **77** (no. 8), 27 (1999).
2. M. A. Unger *et al.*, *Science* **288**, 113 (2000); J. Fahrenberg *et al.*, *J. Micromech. Microeng.* **5**, 169 (1995); C. Goll *et al.*, *J. Micromech. Microeng.* **6**, 77 (1996); X. Yang, C. Grosjean, Y. C. Tai, C. M. Ho, *Sens. Actuators A* **64**, 101 (1998).
3. D. J. Harrison *et al.*, *Science* **261**, 895 (1993).
4. H. Salimi-Moosavi, T. Tang, D. J. Harrison, *J. Am. Chem. Soc.* **119**, 8716 (1997).
5. G. Beni, M. A. Tenan, *J. Appl. Phys.* **52**, 6011 (1981).
6. B. S. Gallardo *et al.*, *Science* **283**, 57 (1999).
7. D. E. Kataoka, S. M. Troian, *Nature* **402**, 794 (1999).
8. M. A. Burns *et al.*, *Proc. Natl. Acad. Sci. U.S.A.* **93**, 5556 (1996).
9. A. W. Adamson, *Physical Chemistry of Surfaces* (Wiley, New York, ed. 5, 1990).
10. J. C. Mcdonald *et al.*, *Electrophoresis* **21**, 27 (2000).
11. K. Handique, B. P. Gogoi, D. T. Burke, C. H. Mastrangleo, M. A. Burns, *Proc. SPIE* **3224**, 185 (1997).
12. E. Delamarche, A. Bernard, H. Schmid, B. Michel, H. Biebuyck, *Science* **276**, 779 (1997).
13. K. Ichimura, S.-K. Oh, M. Nakagawa, *Science* **288**, 1624 (2000).
14. H. Gau, S. Herminghaus, P. Lenz, R. Lipowsky, *Science* **283**, 46 (1999).
15. A. A. Darhuber, S. M. Troian, S. M. Miller, *J. Appl. Phys.* **87**, 7768 (2000).
16. A. D. Strook *et al.*, *Phys. Rev. Lett.* **84**, 3314 (2000).
17. G. T. A. Kovacs, *Micromachined Transducer Sourcebook* (McGraw-Hill, Boston, 1998).
18. B. H. Weigl, P. Yager, *Science* **283**, 346 (1999).
19. P. J. A. Kenis, R. F. Ismagilov, G. M. Whiteside, *Science* **285**, 83 (1999).
20. S. Takayama *et al.*, *Proc. Natl. Acad. Sci. U.S.A.* **96**, 5545 (1999).
21. A. Ulman, *An Introduction to Ultrathin Organic Films* (Academic Press, Boston, 1991).
22. A. Ulman, *Chem. Rev.* **96**, 1533 (1996).
23. B. Zhao, D. Mulkey, W. J. Brittain, Z. Chen, M. D. Foster, *Langmuir* **15**, 6856 (1999).
24. We used hexadecane (Aldrich, 99%) as a solvent to form SAMs of trichlorosilanes on silica substrates. Contact angle measurement showed that SAMs with full coverages were formed on glass substrates in less than 2 min.
25. D. J. Beebe *et al.*, *Nature* **404**, 588 (2000).
26. Hexadecane and the solution of trichlorosilane in hexadecane [0.5 weight-to-volume percent (w/v %)] were pumped into channels by two syringe pumps (Harvard Apparatus PHD 2000 Programmable). Syringes were connected to pipette tips fixed to channels by silicone tubing (Helix Medical, 0.040″ ID/0.085″ OD). Because the reactivity of trichlorosilanes is high, solvent was always introduced into the channel before the silane solution to eliminate the formation of SAMs in unwanted areas. At the end of the process, flow of the silane solution was always halted before stopping the flow of pure solvent. The flow rates of solvent and solution were usually the same, either 1 or 2 ml/min; the flow time was 2 to 3 min. The channels were cleaned by sequentially flushing with 10 ml of hexane and 10 ml of methanol followed by drying with a stream of clean air or nitrogen.
27. A pipette tip with inner diameters of 8 mm at the bottom and 6 mm at the top was fixed onto the channels. The maximum pressure that virtual walls can withstand was determined by gradually adding deionized water into the pipette and then measuring water height when a bulge developed.
28. The surface free energy of Rhodamine B dilute solution is lower than that of deionized water, resulting in a lower maximum pressure.
29. D. H. Rich, S. K. Gurwara, *J. Am. Chem. Soc.* **97**, 1575 (1975); V. N. R. Pillai, *Synthesis (Germany)* (1980), p. 1.
30. S. C. Jacobson, M. Ramsey, *Electrophoresis* **16**, 481 (1995).
31. R. D. Oleschuk, L. L. Shultz-Lockyear, Y. Ning, D. J. Harrison, *Anal. Chem.* **72**, 585 (2000).
32. D. J. Beebe *et al.*, *Proc. Natl. Acad. Sci. U.S.A.* **97**, 13488 (2000).

33. Supported by a grant from the Defense Advanced Research Projects Agency (MTO F30602-00-1-0570) (A. Lee, Program Manager). We acknowledge J. Orlicki for assisting with the images and Q. Yu for help in generating the photomasks.

8 November 2000; accepted 4 January 2001

The Detection of Large HNO_3-Containing Particles in the Winter Arctic Stratosphere

D. W. Fahey,[1,3]* R. S. Gao,[1] K. S. Carslaw,[4] J. Kettleborough,[5] P. J. Popp,[1,3] M. J. Northway,[1,3] J. C. Holecek,[1,3] S. C. Ciciora,[1,3] R. J. McLaughlin,[1] T. L. Thompson,[1] R. H. Winkler,[1] D. G. Baumgardner,[6] B. Gandrud,[7] P. O. Wennberg,[8,9] S. Dhaniyala,[8] K. McKinney,[8] Th. Peter,[10] R. J. Salawitch,[11] T. P. Bui,[12] J. W. Elkins,[2] C. R. Webster,[11] E. L. Atlas,[7] H. Jost,[12,13] J. C. Wilson,[14] R. L. Herman,[11] A. Kleinböhl,[15] M. von König[15]

Large particles containing nitric acid (HNO_3) were observed in the 1999/2000 Arctic winter stratosphere. These in situ observations were made over a large altitude range (16 to 21 kilometers) and horizontal extent (1800 kilometers) on several airborne sampling flights during a period of several weeks. With diameters of 10 to 20 micrometers, these sedimenting particles have significant potential to denitrify the lower stratosphere. A microphysical model of nitric acid trihydrate particles is able to simulate the growth and sedimentation of these large sizes in the lower stratosphere, but the nucleation process is not yet known. Accurate modeling of the formation of these large particles is essential for understanding Arctic denitrification and predicting future Arctic ozone abundances.

Polar stratospheric cloud (PSC) particles play a well-recognized role in the chemical loss of stratospheric ozone over the Antarctic and Arctic regions in winter/early spring (*1–3*). PSCs are formed at low temperatures (<200 K), characteristic of the winter stratosphere, through the co-condensation of water and HNO_3. Heterogeneous reactions on PSC particles produce active chlorine species. The sedimentation of PSC particles irreversibly removes HNO_3 (denitrification) and water (dehydration) from the lower stratosphere. Denitrification slows the return of chlorine to its inactive forms and, hence, enhances ozone destruction in a winter/spring season (*4–6*).

Evidence of denitrification is abundant in both polar stratospheres from both in situ and remote observations (*2, 7–11*). Denitrification is most intense over the Antarctic region, where large fractions of available NO_y are irreversibly removed from the stratosphere each winter. NO_y is the sum of principal reactive nitrogen species, of which HNO_3, NO, NO_2, N_2O_5, and $ClONO_2$ are important in the lower stratosphere (*12*). In principle, denitrification must involve the sedimentation of large HNO_3-containing particles (*13, 14*), but important details of the process have not been confirmed by observation or fully described theoretically. The concentration of denitrifying particles must generally be much less than that of the background liquid sulfate aerosols (0.1-μm diameter). Too little condensable material (HNO_3, H_2O) exists in the stratosphere to allow all particles to grow simultaneously to sizes sufficient for rapid sedimentation, particularly when ice does not form.

Here we report observations in the Arctic winter stratosphere of a newly identified class of large HNO_3-containing particles. The particles were observed between January and